Enhancing Prediction Accuracy and Mitigating Structural Dependencies in Curvilinear EUV Mask Patterning with Hybrid Parametric PSF Models

C.H. Liu*, Y.J. Zhong, H.C. Tai, S.K. Hsu, Z.A. Ding, S.W. Hsu, S.K. Wong, Y.L. Chung, Y.H. Tu, Y.C. Li, Y.T. Sun
Department of Electrical Engineering, National Taipei University, Taipei, Taiwan
**E-mail: chliuzzh@mail.ntpu.edu.tw*

Extreme ultraviolet (EUV) lithography, as the most advanced technology currently, faces limitations with conventional (conv.) parametric point spread function (PPSF) models due to the complex mask structures. These models fail to meet the precision requirements for 2 nm and more advanced nodes. To address this issue, several hybrid PPSF models are proposed, combining Gaussian, exponential, and Lorentz distribution components[1]. Compared to conv. triple-Gaussian (BSL_A) and three-exponential (BSL_B) PPSF models, the new models enhance precision, better represent electron scattering over different ranges, overcome limitations in accuracy, and improve the correlation between curve fitting (CF) and pattern prediction[2] (PP) accuracy. Fig. 1 shows the simulation conditions of electron beam lithography in this study, with (a) illustrating the mask structures of binary intensity mask (BIM) and alternating phase shift mask (AltPSM). Fig. 1(b) shows the expressions of baselines (BSL) and optimized (Opt.) PPSFs, where α, β, γ, η, and η' are coefficients representing the radial distance from the incident beam, forward scattering (FS) range, backscattering (BS) range, the intermediate region between FS and BS, relative intensity ratio of the BS region to the FS region, and the relative intensity ratio of the intermediate region to the FS region, respectively. Fig. 1(c) provides three merit functions of CF to obtain determined-optimal coefficients. Fig. 2(a1) represents the fitting results with Opt. merit functions, PPSFs, BSLs, and AED with EUV-BIM. Fig. 2(a2) to (a4) show curves divided into four segments: short range (SR), middle range (MR), long range (LR), and ultra-long range (ULR) for EUV-BIM. These ranges are determined by LogNSSE function fit coefficients (α, β, and γ) of the triple-Gaussian model, which reduces the impact of extreme values on results. The fitting results exhibit a high fitting performance of the EG + L form compared to BSLs. Fig. 2(b) shows the line-bar combined chart illustrating the CF performance of the proposed PPSFs and BSLs for both structures, quantified by R^2 and root mean square error (RMSE) performance index (PI). The BSL_A fitting performance is inferior to the other forms. Fig. 2(c1) and (c2) are line charts showing CF segment (Seg.) PI, which is the normalized mean value of R^2 and RMSE PI in different PPSFs with both structures, and exhibit overall CF PI related to SR and MR PI. Fig. 3 relates to PP, with schematic diagrams illustrating isolated (ISO) and 75% pattern density (PD 75%) (a1) line and space (L/S) patterns, and (a2) via layers, with their regions of interest (ROI) analyzed. Fig. 3(b1) and (b2) depict ROI 1 and 2 of curvilinear 1 and 2 (CL 1, CL 2). Fig. 3(c1) to (c4) depict the correlation coefficient (corr.) analysis between the mean normalized CF PIs and PP ROI-PI [EPE mean], based on the r-value magnitude. Fig. 3(c1) reveals that rectilinear patterns exhibit higher corr. compared to CL 1 and CL 2, suggesting that CF and PP results are less consistent in CL patterns due to varying degrees of proximity effects, ROI curvature, pattern density, and the presence of sub-resolution assistant features (SRAFs). Fig. 3(c2) and (c3) depict the corr. with two mask structures in CL 1 and CL 2. Fig. 3(c2) shows that the corr. in CL 2 is lower for BIM, while Fig. 3(c3) further analyzes the same ROIs of CL 1 and CL 2, where the low corr. appears only in BIM. Fig. 3(c4) depicts corr. between PP ROI-PP and CF Seg. PI, showing that severe proximity effect ROIs have a strong corr. with MR and LR PI compared to SR and ULR. In Table I and II, the green boxes indicate accuracy improvements, the soft pink purple backgrounds indicate accuracy declines, and the pastel yellow backgrounds represent the reasons for these declines. The results in Table I and II show that to improve PP accuracy for CL patterns, the fitting accuracy in MR and LR must be prioritized during PPSF optimization. Accurate CF is critical for enhancing PP precision and aligning PP and CF results, as supported by Fig. 3(c4). Opt. PPSFs outperform conv. PPSFs in CF, with a high corr. between CF and PP results for rectilinear patterns. However, this is not the case for CL patterns. High-precision results are achieved when CF in MR and LR exhibits better corr. than conv. PPSFs. Additionally, PPSFs exhibit structural dependence: EG + L is more suitable for fitting BIM AED, while G + E combinations are more suitable for fitting AltPSM AED.

---

[1] Thiago Rosa Figueiro, *Université Grenoble Alpes*, 2015

[2] C. H. Liu et. al., in *J. Vac. Sci. Technol. B* 31, 2021605 (2013)

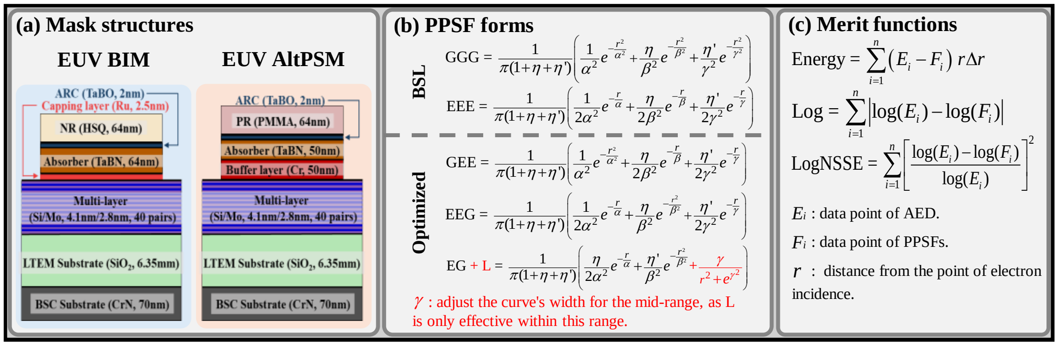

Fig. 1: (a) EUV BIM and AltPSM structures. (b) Conventional (BSL) and optimized PPSF forms for curve fitting (CF). (c) Merit functions used to evaluate fitting quality.

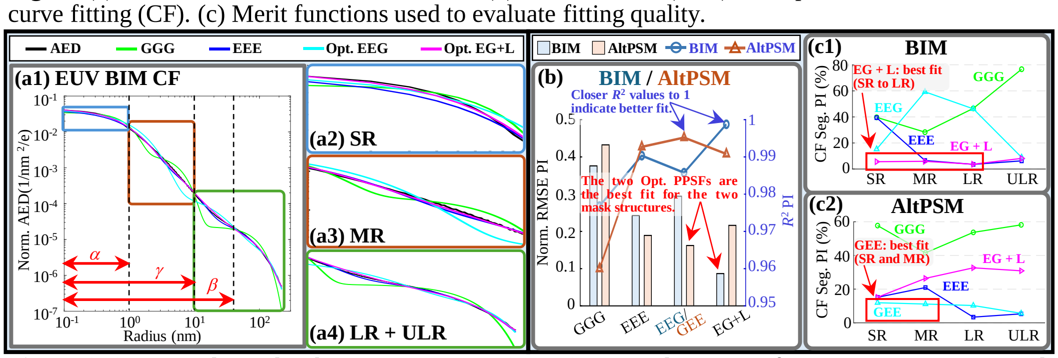

Fig. 2: (a1) CF results under the BIM structure. (a2–a4) Zoomed-in views for SR to ULR, segmented by LogNSSE fit coefficients (α, γ, and β) of GGG model. (b) Comparison of CF PI between BIM and AltPSM. (c1) CF Seg. PI for BIM and (c2) AltPSM across different ranges.

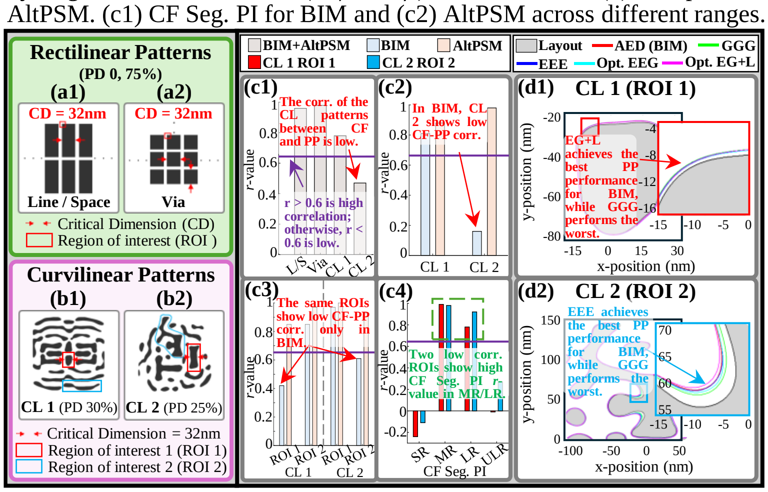

🡐 **Fig. 3:** (a1–a2, b1–b2) show the test pattern info. (c1) presents average CF and PP correlations for two mask structures. (c2) compares CL patterns between the two mask structures. (c3) examines CF and PP correlations for ROI 1 and 2. (c4) analyzes the correlation between CF Seg. PI and PP results in low-correlation ROIs. (d1) and (d2) illustrate contours for CL 1 in ROI 1 and CL 2 in ROI 2 (zoomed-in views.)

Table I and II Comparison of CF and PP PIs for conventional (BSL) and optimized PPSF forms.

Declines explained BIM / AltPSM CF Performance Index		GGG / GGG Energy / Energy fit (BSL_A)	EEE / EEE Energy / Log fit (BSL_B)	Opt. EEG / GEE Log / Energy fit Value	Impro. (vs. BSL_A)	Impro. (vs. BSL_B)	Opt. EG + L / EG + L LogNSSE / Energy fit Value	Impro. (vs. BSL_A)	Impro. (vs. BSL_B)
SR	RMSE (×10^{-5})	417 / 204	264 / 84.3	208 / 70.4	21% / 29%	6% / 3%	93.4 / 103	33% / 22%	17% / -4%
MR	RMSE (×10^{-5})	81.2 / 28.5	31.7 / 17.3	136 / 10.5	-20% / 30%	-38% / 11%	26.5 / 3.50	20% / 42%	2% / 23%
LR	RMSE (×10^{-5})	3.98 / 1.29	0.56 / 0.12	3.86 / 0.34	1% / 50%	-37% / -11%	0.57 / 0.15	38% / 60%	0% / -2%
ULR	RMSE (×10^{-5})	0.09 / 0.04	0.02 / 0.01	0.02 / 0.01	49% / 53%	-3% / -1%	0.02 / 0.01	50% / 45%	-3% / -9%
Overall	R^2	0.98 / 0.96	0.99 / 0.99	0.99 / 1.00	25% / 67%	0% / 17%	1.00 / 0.99	50% / 50%	25% / 0%
Overall	RMSE (×10^{-5})	32.2 / 16.3	20.8 / 6.95	25.2 / 5.64	8% / 27%	-5% / 3%	7.43 / 7.80	29% / 22%	16% / -3%
					Accuracy improved			Accuracy improved	

Accuracy declined BIM / AltPSM EPE$_{mean}$ (nm)		AED	GGG / GGG Energy / Energy fit (BSL_A)	EEE / EEE Energy / Log fit (BSL_B)	Opt. EEG / GEE Log / Energy fit Value	Impro. (vs. BSL_A)	Impro. (vs. BSL_B)	Opt. EG + L / EG + L LogNSSE / Energy fit Value	Impro. (vs. BSL_A)	Impro. (vs. BSL_B)
L/S	ROI	1.52 / 1.07	2.17 / 1.18	1.67 / 1.13	1.17 / 1.08	20% / 9%	-13% / 5%	1.53 / 1.12	42% / 6%	9% / 2%
Via	ROI	0.46 / 0.68	0.76 / 0.83	0.55 / 0.77	0.33 / 0.71	40% / 18%	-8% / 9%	0.45 / 0.66	65% / 17%	18% / 9%
CL 1	ROI 1	0.67 / 0.78	0.65 / 0.87	0.67 / 0.83	0.6 / 0.81	-7% / 8%	-10% / 2%	0.67 / 0.79	3% / 10%	0% / 5%
CL 1	ROI 2	0.61 / 1.42	0.77 / 1.12	0.68 / 1.39	0.56 / 1.46	19% / 18%	5% / -1%	0.63 / 1.54	22% / 12%	9% / -7%
CL 2	ROI 1	0.61 / 0.84	0.48 / 1.01	0.58 / 0.86	0.53 / 0.84	8% / 96%	-8% / 2%	0.62 / 0.87	20% / 17%	78% / -1%
CL 2	ROI 2	1.07 / 1.35	0.95 / 1.53	1.04 / 1.33	0.88 / 1.37	-6% / 87%	14% / -1%	1.11 / 1.44	7% / 6%	-28% / -6%
						Accuracy improved			Accuracy improved	